Int. J. Heat Mass Transfer. Vol. 27, No. 3, pp. 351–361, 1984
Printed in Great Britain

0017–9310/84 $3.00 + 0.00

STUDY OF LIQUID SPRAY (WATER) IN A NON-CONDENSABLE ENVIRONMENT (AIR)

S. Y. LEE* and R. S. TANKIN
Department of Mechanical and Nuclear Engineering, Northwestern University, Evanston, IL 60201, U.S.A.

(*Received* 29 *June* 1982 *and in revised form* 13 *June* 1983)

Abstract—A model to describe the behavior of a water spray in an air environment is proposed. For modeling purposes, the spray is divided into two regimes—sheet portion and droplet portion. The sheet portion is important in determining the spray angle. A relation between sheet length and Weber number is obtained. The computed trajectory of droplets is substantiated qualitatively by measurements using an oil bath to capture the droplets.

NOMENCLATURE

a	constant
$\bar{a}$	distribution parameter
A	constant
A_0	flow area of nozzle [m^2]
b, c_1, c_2	constants
c_D	drag coefficient
D	drop diameter [μm]
D_m	maximum drop diameter [μm]
D_n	equivalent orifice diameter [m]
L	breakup length
$\dot{m}_L$	mass flow rate of liquid [kg s^{-1}]
N	number of drops
P	pressure of gas inside the water sheet [N m^{-2}]
P_o	pressure of gas outside the water sheet [N m^{-2}]
ΔP	pressure difference, $P-P_o$
Q	volume flow rate of liquid [m^3 s^{-1}]
r	radial distance from the axis [m]
t	water sheet thickness [m]
T_L	temperature of liquid [°C]
u	velocity of liquid along streamline [m s^{-1}]
V	volume of droplets
V_0	velocity difference, $\sqrt{[(V_{L,z}-V_{g,z})^2+(V_{L,r}-V_{g,r})^2]}$
$V_{L,r}$	velocity of liquid in radial direction [m s^{-1}]
$V_{L,z}$	velocity of liquid in axial direction [m s^{-1}]
$V_{g,r}$	velocity of gas in radial direction [m s^{-1}]
$V_{g,z}$	velocity of gas in axial direction [m s^{-1}]
We	Weber number
z	axial distance from nozzle [m].

Greek symbols

δ	distribution parameter
ζ	radius of curvature [m]
θ	time [s]
ρ_g	gas density [kg m^{-2}]
ρ_L	liquid density [kg m^{-3}]
σ	surface tension [N m^{-1} or dyne cm^{-1}]
ϕ	$\tan^{-1}(dr/dz)$
ψ	stream function.

* Present address: Department of Mechanical Engineering, Korea Advanced Institute of Science and Technology, Seoul, Korea.

1. INTRODUCTION

SPRAYS have many engineering applications; for example, sprays are used in combustion systems, in direct contact condensers, etc. The main idea of these sprays is to increase the surface area of the injected liquid, thereby increasing the heat and mass transfer rates. We will examine a liquid spray in a non-condensable media in this paper (Paper I) in order to clarify the problem. In the following paper (Paper II), we will examine the spray in a condensable medium and explain the differences.

Over the years, numerous research has been conducted on sprays dealing with the breakup mechanism, the effects of ambient pressure, injection pressure and liquid properties [1–10]. Giffen and Muraszew [11], and Reitz [12] as well as others, have written extensive reviews on sprays.

Examples of models proposed to describe the breakup mechanism are given by Castleman [13], Schweitzer [14], and Dombrowski and co-workers [15–20]. Castleman concluded that the atomization of jets is due to the drag of the ambient gas; the jet is drawnout—resulting in fine drops due to Rayleigh instability. Schweitzer speculated that the breakup mechanism is caused by turbulent motion which occurs inside the nozzle. The radial disturbance (velocity fluctuations) tends to breakup the interface as soon as the restraint imposed by the orifice wall ceases. Dombrowski concluded two principal modes of disintegration—aerodynamic instability and perforations. The aerodynamic instability is due to interfacial surface tension and aerodynamic forces. These aerodynamic forces result in a Kelvin–Helmholtz type instability. Perforations are assumed to be caused by either non-wettable particles or turbulence. There are no quantitative calculations which clearly substantiate these proposed breakup mechanisms.

Rothe and Block [21] proposed a simple one-dimensional (1-D) model to compute the spray angle. In this analysis the drop size is assumed uniform and

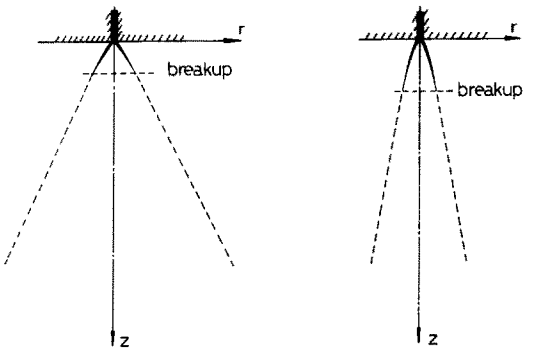

FIG. 1. Effect of breakup length and shape of spray sheet on final shape of the spray.

breakup is assumed to be complete at injection. There are some review works on the measurements of drop size, such as in ref. [22], and several mathematical expressions have been proposed for fitting the droplet distribution curve in refs. [23, 24]. They concluded that the upper-limit function fits the droplet distribution best and is simple to use.

In the present study the behavior of a spray will be examined in detail—including the water sheet region, breakup point, and droplet region. A model is presented and numerical results are compared with experiments. Usually the nozzles used in direct contact condensation are wide angle sprays—which are classified as hollow cone sprays. We will confine our attention to hollow cone sprays which are generated by either swirl nozzles or poppet type nozzles. The experiments involve normal photography, holography, and the capture of droplets in an oil bath.

2. ANALYTICAL MODEL

2.1. *Sheet portion of spray*

It has been found in our experiments, that the sheet portion—its shape and breakup length—plays a major role in determining the outline of the spray (see Fig. 1). Up to the breakup point, the sheet can be regarded as a special case of a water bell. Taylor [25] worked on this problem extensively—both analytically and experimentally. Referring to Fig. 2, the governing equation for the sheet portion is

$$\frac{2\sigma}{\zeta}+\frac{2\sigma\cos\phi}{r}-\Delta P+\rho_L g t\sin\phi-\frac{\rho_L u^2 t}{\zeta}=0, \quad (1)$$

where σ is the surface tension, t the water sheet thickness, ζ the radius of curvature, ΔP the pressure difference between the inside and outside of the sheet, $P-P_o$, and u is the velocity along the streamline. It should be noted that in this study, we are not considering the swirl nozzle; although the theory has been extended to include swirl nozzles [29] and will be included in Paper II. Usually the gravitational force is negligible and the velocity of the water in the sheet is nearly constant. Therefore, the gravitational term in equation (1) will be neglected.

$$Q=2\pi r u t, \quad (2)$$

where Q is the volume flow rate.

Taylor solved equation (1) neglecting ΔP. However, because of the motion of air inside the sheet region, ΔP may not be negligible. Parlange [26] computed the effect of internal airflow on the shape of a water bell and found it was not negligible. Figure 3 shows the expected flow of air around the water spray as well as inside the sheet portion. Closed streamlines will be formed inside the sheet portion—driven by the drag of the water sheet. Air is entrained from the surroundings due to the pumping effect of the droplets at breakup. The motion of the air circulation inside the sheet region was studied, following the approach of Parlange, to determine its significance on the shape of the sheet region of the spray. The assumed airflow pattern is substantiated quantitatively by simple experiments. Assuming the air to be incompressible, and the flow to be axisymmetric and non viscous; a stream function of the form

$$\psi=\frac{Ar^2}{8+16ab/3}\left[r^2(1+ab-za)-\tfrac{4}{3}az^2(b-z)\right], \quad (3)$$

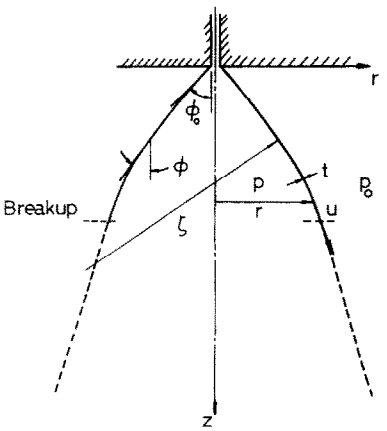

FIG. 2. Simplified shape of spray sheet used for calculations

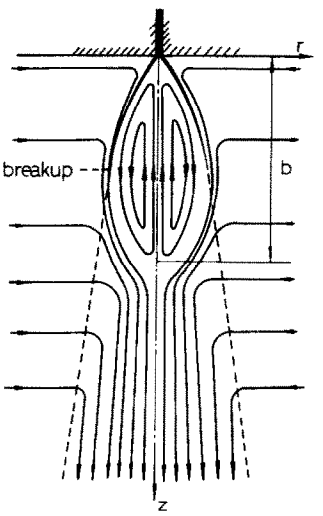

FIG. 3. Expected flow pattern of air around the water spray.

is selected which satisfies the momentum equations. The shape of the water sheet is denoted by $\psi = 0$. The r and z directional velocities of gas inside the water sheet will be

$$V_{g,r} = \frac{1}{r}\frac{\partial \psi}{\partial z}, \tag{4}$$

$$V_{g,z} = -\frac{1}{r}\frac{\partial \psi}{\partial r}, \tag{5}$$

and the pressure difference (ΔP) at $\psi = 0$ will be

$$\Delta P = \tfrac{1}{2}\rho_g[V_{g,r}^2 + V_{g,z}^2]. \tag{6}$$

By determining the stagnation point (b) and the velocity at one point experimentally, the values of A and a are found from the best fit of equation (1) by iteration.

2.2. *Droplet portion of spray*

In the droplet portion of the spray, the liquid droplets entrain the surrounding air. As the air moves inwards a drag force develops on the droplets; thus decreasing the spray cone angle. The behavior of the droplets are computed with the following assumptions:

(a) all droplets are spherical;
(b) the droplets have a size distribution which can be represented by an upper-limit function;
(c) the velocity of the droplets at the breakup point are assumed to be the same as the sheet velocity at the breakup point;
(d) the pressure in the droplet region is assumed to be uniform and equal to the ambient pressure;
(e) no interaction occurs between droplets, i.e. no secondary breakup or coalescence;
(f) gravity force is neglected.

The equation for the drop size distribution (upper-limit function) is given by Mugele and Evans [23]

$$y = \ln\left[\frac{\bar{a}D}{D_m - D}\right], \tag{7}$$

$$\frac{dV}{dD} = \frac{\delta}{\sqrt{\pi}}\frac{D_m}{D(D_m - D)}\exp(-\delta^2 y^2), \tag{8}$$

where D is the drop diameter, D_m the maximum drop diameter, and $\bar{a}$ and δ are distribution parameters.

The number of droplets produced per unit time with a diameter between $D + 1/2dD$ and $D - 1/2dD$ is

$$dN = \frac{\dot{m}_L}{\rho_L}\frac{\delta}{\sqrt{\pi}}\frac{D_m}{D(D_m - D)}\frac{6}{\pi D^3}\exp(-\delta^2 y^2)\,dD. \tag{9}$$

The force balance on the droplet yields

$$\frac{dV_{L,z}}{d\theta} = -\frac{3}{4}\frac{C_D}{D}\frac{\rho_g}{\rho_L}V_0(V_{L,z} - V_{g,z}), \tag{10}$$

$$\frac{dV_{L,r}}{d\theta} = -\frac{3}{4}\frac{C_D}{D}\frac{\rho_g}{\rho_L}V_0(V_{L,r} - V_{g,r}), \tag{11}$$

where

$$V_0 = [(V_{L,z} - V_{g,z})^2 + (V_{L,r} - V_{g,r})^2]^{1/2}. \tag{12}$$

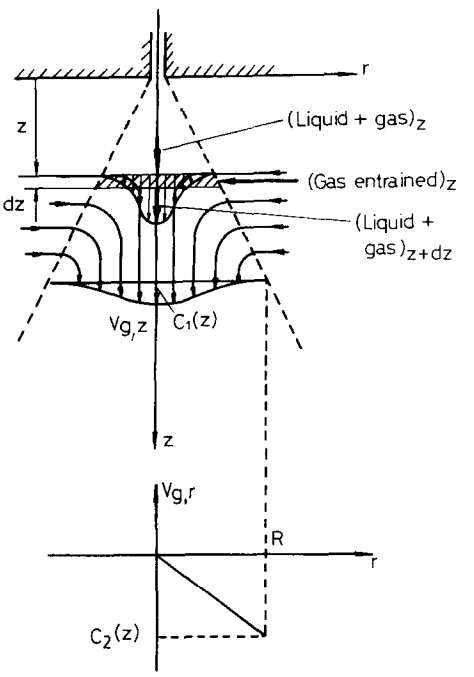

FIG. 4. Vapor velocity profile model used at the droplet portion of the spray.

The drag coefficient (C_D) is chosen from ref. [27]—where C_D is given as a function of Reynolds number. The effect of evaporation on C_D was determined by Yuen and Chen [28].

A momentum balance (z-direction) on the spray-droplets and gas (in this case, air) yields

$$\underbrace{\int_D \frac{\pi}{6}D^3\rho_L V_{L,z}\,dN}_{\text{momentum of droplets}} + \underbrace{\int_R \rho_g 2\pi r V_{g,z}^2\,dr}_{\text{momentum of gas}} = \text{const.} \tag{13}$$

The velocity profile of the vapor is assumed to be similar to that of a free circular jet. This is shown schematically in Fig. 4. An approximate mathematical expression for such a profile is

$$V_{g,z} = C_1(z)\left(1 + \frac{r}{R}\right)^2\left(1 - \frac{r}{R}\right)^2, \tag{14}$$

$$V_{g,r} = -C_2(z)\frac{r}{R}, \tag{15}$$

where $C_1(z)$ is the centerline velocity of the gas, $C_2(z)$ is the radial velocity of the gas at the spray boundary, and R is the radius of the spray. Other power relations were assumed for the gas velocity profiles and they had little effect on the computed path lines of the droplets. For example, $V_{g,z} = C_1(1 + r/R)^2(1 - r/R)^2(r/R)^2$ was assumed. This profile has zero velocity at the center and edge of the spray with a maximum within the spray. Another profile assumed was a constant velocity profile; that is, $V_{g,z} = C_1(z)$.

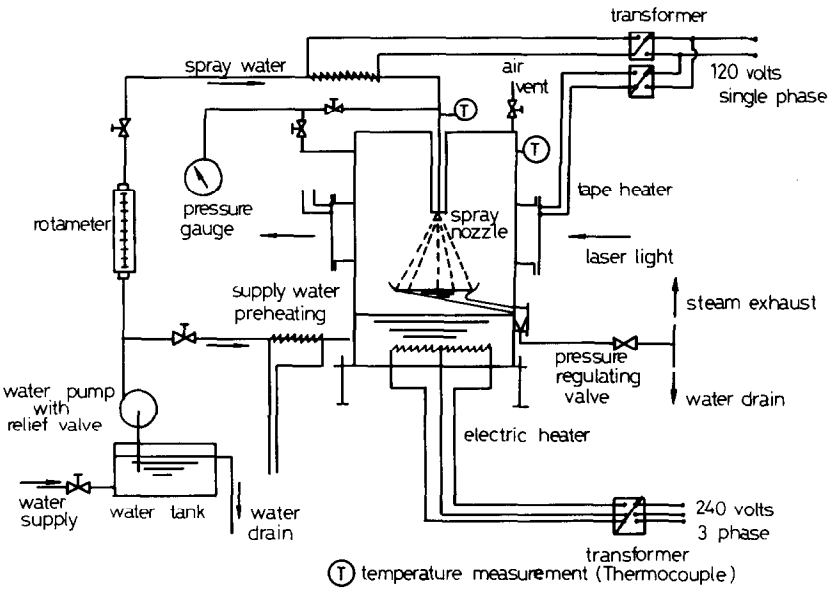

FIG. 5. Schematic diagram of the experimental system.

The mass flux of the gas is balanced as

$$2\pi R\rho_g V_{g,r}\,dz = \int_0^{R+dR} 2\pi r\rho_g (V_{g,z})_{z+dz}\,dr - \int_0^R 2\pi r\rho_g (V_{g,z})_z\,dr. \quad (16)$$

The velocity and position of droplets will be determined from

$$(V_{L,z})_{z+dz} = (V_{L,z})_z + \left(\frac{dV_{L,z}}{d\theta}\right)_z (d\theta)_z, \quad (17)$$

$$(V_{L,r})_{z+dz} = (V_{L,r})_z + \left(\frac{dV_{L,r}}{d\theta}\right)_z (d\theta)_z, \quad (18)$$

$$(R)_{z+dz} = (R)_z + (V_{L,r})_z (d\theta)_z, \quad (19)$$

$$dz = (V_{L,z})(d\theta). \quad (20)$$

Using these equations the trajectory of the droplets can be computed.

3. EXPERIMENTS

3.1. *Experimental set-up*

A schematic diagram of the experimental set-up is shown in Fig. 5. The electric heaters in the test chamber were not used in these experiments where the environment is air. In this study, the test chamber is maintained at atmospheric pressure; however, the test chamber is designed so that its pressure can be set at a pre-selected value between 1 and 3 atm.

A gear pump supplies tap water to the spray nozzle. The spray water flow rate is measured with a calibrated rotameter. Heating tape is wrapped around the water inlet pipe; thus, allowing one to control the temperature of the water. A poppet type nozzle was used, which was constructed in the departmental machine shop to our design. A schematic diagram of this nozzle is shown in Fig. 6.

Experimental data on spray shape and droplet size distribution were obtained from holograms and normal photography. A schematic drawing of the off-axis holographic set-up is shown in Fig. 7. For normal photography the laser reference beam was blocked and the pulsed laser acted as a light source (back lighting) and shutter. The pulse duration is approximately 8–9 ns. Holography was used to obtain the droplet size distribution as well as determining the shape of the

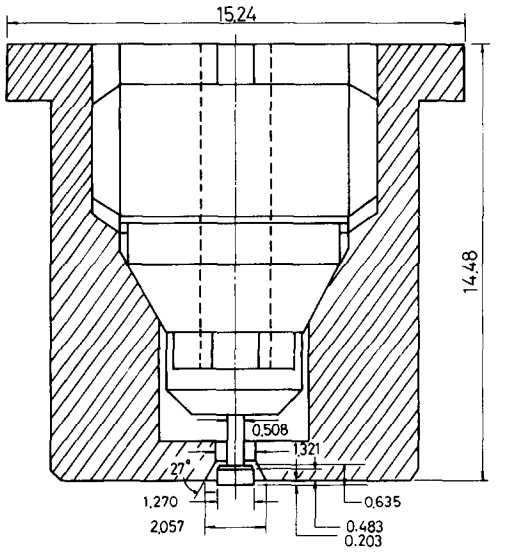

FIG. 6. Schematic diagram of the poppet type nozzle used in the experiments.

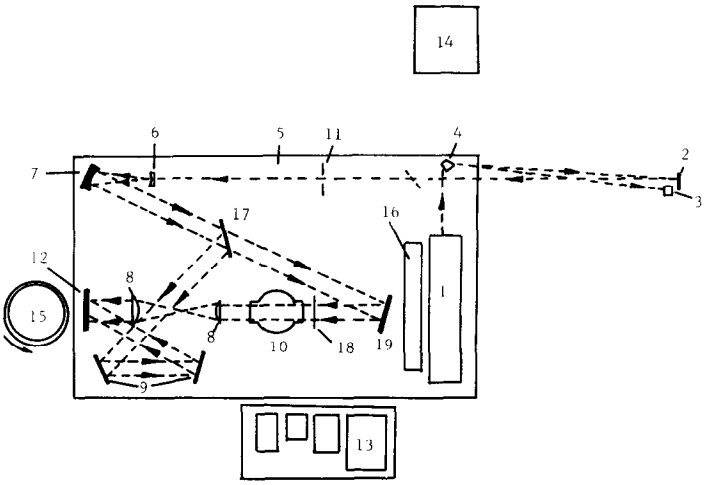

FIG. 7. Schematic diagram of off-axis holographic set-up: (1) Nd : YAG laser; (2) folding mirror; (3) infrared trap (1.06 μm); (4) prism; (5) vibration isolated table; (6) plano-concave lense; (7) off-axis paraboloid mirror; (8) focusing lenses; (9) plane folding mirrors; (10) test section; (11) variable iris stop; (12) holographic plate; (13) ELN line-width narrower; (14) laser power supply; (15) turn table; (16) He–Ne laser (for reconstruction); (17) beam splitter; (18) ground glass diffuser; (19) plane mirror (for objective beam).

sheet portion; normal photography was used to determine the spray angle.

3.2. *Sheet portion of spray*

It is difficult to measure the velocity of the air inside the sheet portion of the spray by conventional methods because of space limitations and fog generated by the spray itself. It was noticed that when a thin needle is placed vertically inside the sheet region (along the centerline of the spray), a stationary droplet formed on the needle which grew in size (see Fig. 8). This droplet is formed by condensation of the surrounding fog. If the needle is moved up and down the droplet remained fixed in space. Since the droplet is fixed relative to the flow field when the needle is moved vertically, the surface tension forces are small relative to the gravity and drag forces (the needle may be coated with a thin film of water since it is in a foggy atmosphere). Thus, the upward drag force on the stationary droplet is balanced by the downward gravity force; that is

$$\frac{\pi}{6}D^3\rho_L g = \tfrac{1}{2}C_D\rho_g\left(\frac{\pi}{4}D^2\right)V_{g,z}^2. \tag{21}$$

The velocity of air (at the droplet location) can be computed by measuring the diameter of the droplet and selecting C_D from ref. [27]. The calculated results of the relation between air velocity and droplet diameter is presented in Fig. 9. If the needle is not inserted along the centerline, but near the edge of the sheet (Fig. 10), no such stationary droplet appears. Figure 10 shows

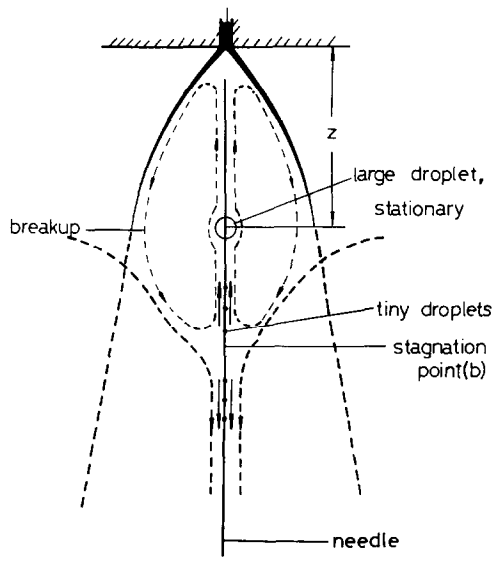

FIG. 8. Schematic diagram of droplets that form on a vertical needle inserted inside the water sheet region.

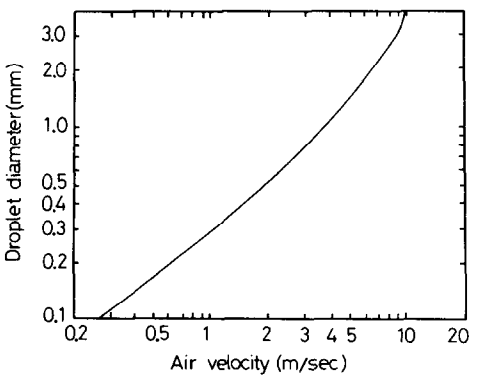

FIG. 9. Relation between air velocity and droplet diameter (ambient pressure is 1 atm).

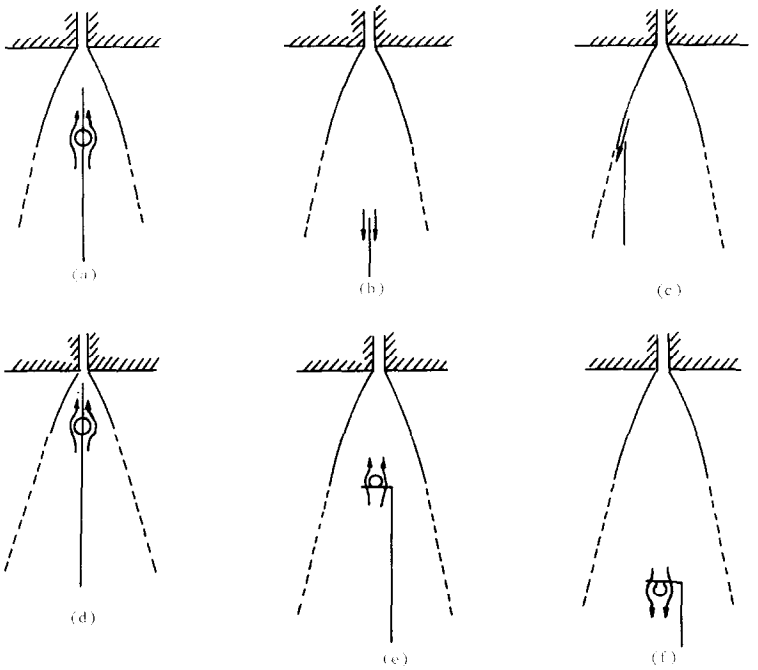

FIG. 10. Schematic diagram of experiments on air/steam flow pattern : (a) needle at center-vertical position ; (b) needle position is lowered (no droplet stays) ; (c) needle position is moved to the edge (no droplet stays) ; (d) water flow rate increased (sheet portion becomes shorter, droplet stays at higher position) ; (e) needle at center-horizontal position (droplet stays on upper side) ; (f) needle at center-horizontal, position lowered (droplet stays on lower side).

schematically the formation of droplets on the needle for different locations of the needle and orientation of the needle (vertical or horizontal).

The stagnation point can be determined by observing the motion of tiny droplets on the needle (when at the spray centerline position). These tiny droplets are moving upward and downward on either side of the stagnation point (see Fig. 8). Figure 11 shows a typical photograph of the needle corresponding to the schematic diagram in Fig. 8.

Surface tension is an important fluid property that is needed to compute the shape of the liquid sheet as well as define the breakup region. In these experiments tap water, whose surface tension may be much lower than distilled water, is used. Thus, it was necessary to measure the surface tension of the tap water if the computed results are to be compared with experiments. Surface tension was determined from 36 photographs of water bells (using Parlange's method). The results are shown in Fig. 12 where a straight line was drawn relating surface tension to temperature. The dotted line above the data points is the surface tension for pure water. The surface tension for the water used in these experiments can be evaluated from the relation

$$\sigma = 60.3 - 0.166 T_L, \tag{22}$$

where σ is the surface tension (dyne cm^{-1}) and T_L is the water temperature (°C). By measuring the meniscus shape (height and width) of the water surface at a vertical wall which is partially immersed in the water bath, the surface tension can also be obtained. This was done as an independent check (at room temperature) and it agreed with the water bell measurements (see Fig. 12).

3.3. *Breakup point*

The location of the breakup point plays an important role in the shape of the water sheet region and thus the overall spray angle. For example, if there is no breakup, a water bell is formed and the resulting spray angle for a poppet nozzle would be very small. Although the breakup of the sheet portion has been studied by many researchers, its value has not been determined analytically. In this study, the breakup point (length of sheet region) is correlated with the Weber number. The correlation obtained is shown in Fig. 13 for the water spray in an air environment. The data can be fitted with an expression of the form

$$\frac{L}{\sqrt{A_0}} = C_1 We^{C_2}, \tag{23}$$

where

$$C_1 = 2.5, \quad C_2 = 0.30 \quad \text{for} \quad We < 750,$$

$$C_1 = 200, \quad C_2 = -0.37 \quad \text{for} \quad We > 750,$$

and L and A_0 are the breakup length and flow area at the nozzle exit, respectively. The curve has a maximum which can be explained as follows. At very low velocities (low Weber number) droplets form at the nozzle tip ; at

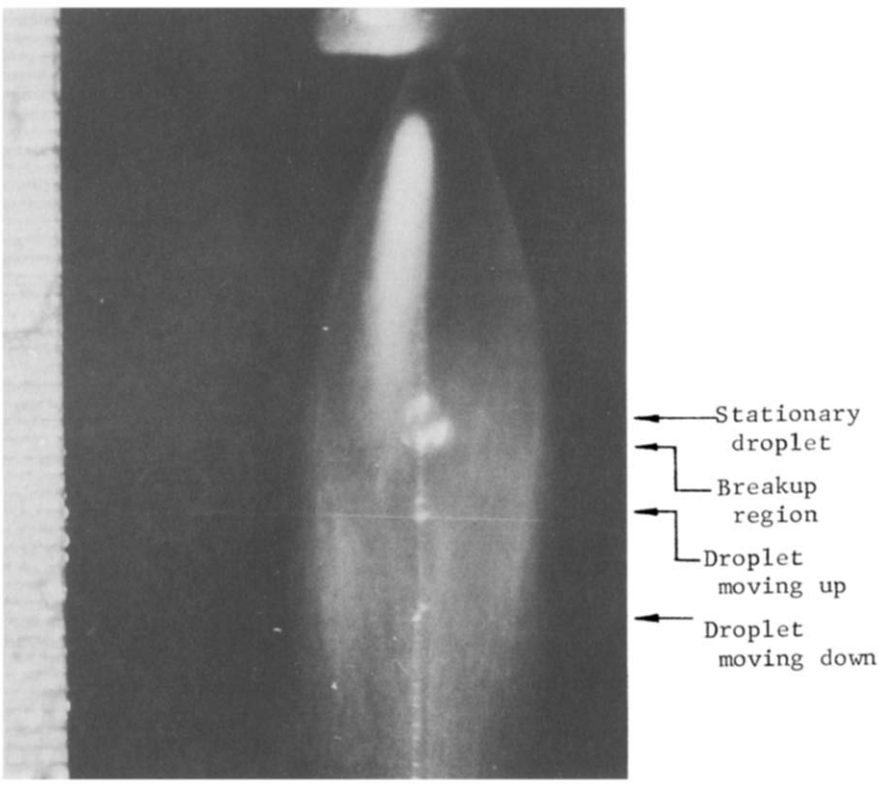

FIG. 11. Photograph of droplets formed on vertical needle inserted inside the water sheet region: $Q = 7.0$ ml s^{-1}; air = 1 atm.

high velocities when the flow in the sheet is turbulent, the breakup length is again short. Thus at intermediate velocities (Weber number) one would expect a maximum to occur. This is born out by experiments (more data points are given in Paper II).

3.4. *Droplet portion of spray*

To compute the trajectories of the droplets after breakup, the droplet size distribution must be determined. There are several methods for measuring the droplet size distributions: oil bath, normal photography, laser scattering, holography, etc. Their advantages and disadvantages are explained in ref. [22]. Holography was used to obtain the droplet size distribution in the neighborhood of the breakup region. A 'best fit' of equations (7) and (8) to the experimental data is made. Using equations (9)–(20), the droplet trajectories can be computed. To check the computations of these droplet trajectories, an oil bath is used to capture the water droplets about 160 mm downstream of the nozzle. There are two reasons for not using holography for these measurements. (1) These measurements would have required enlargement of the test section and thus modification in the holographic

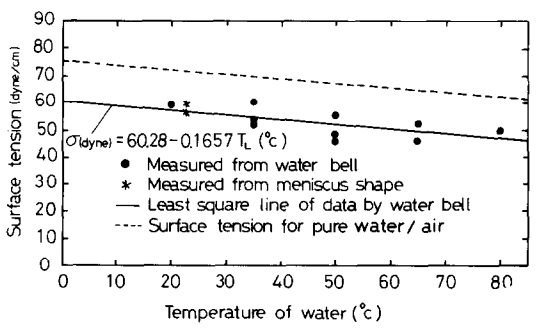

FIG. 12. Surface tension of air/tap water as a function of temperature.

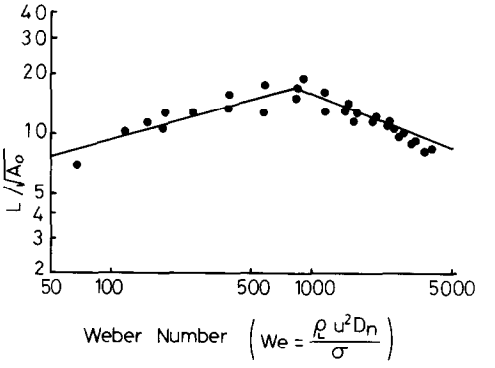

FIG. 13. Breakup length as a function of Weber number.

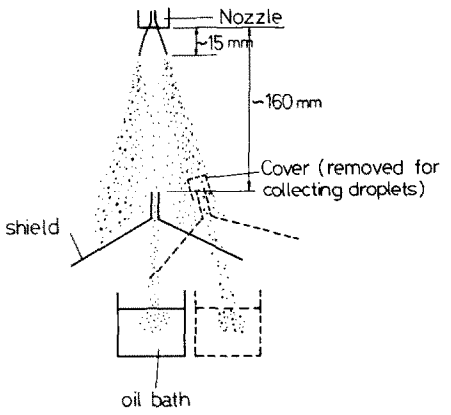

FIG. 14. Schematic configuration of droplet collecting system.

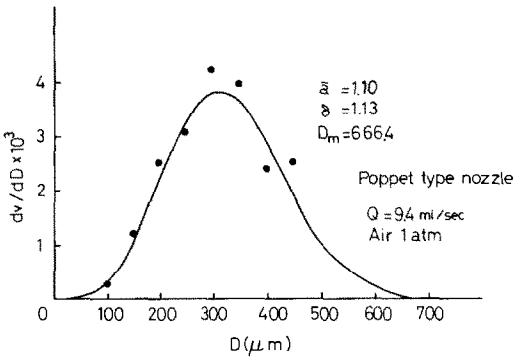

FIG. 16. Plot of the drop size distribution.

setup. (2) The nozzles used in this study are of the hollow cone type. In this type of nozzle the number of droplets per unit volume along the centerline of the spray is much smaller than along the outer edges; thus, holography would have required the analysis of many holograms in order to obtain a meaningful statistical measurement of droplets in the central portion of the spray. The set-up for the oil bath measurement is shown in Fig. 14. The shield is open for a brief period (approximately 1 s) when it is placed at the outer edge of the spray, and for a period of about 10 s when at the centerline. A photograph is then taken of the oil bath and droplet sizes can be determined.

4. SAMPLE CALCULATIONS

Sample calculations for a poppet type nozzle (see Fig. 6) and comparison with experimental results for this nozzle are presented. Similar experiments and calculations were performed with two swirl nozzles and another poppet nozzle of a different size [29]. Flow rates were varied as well as the water inlet temperature. For a typical case under consideration, the flow rate is 6.3 ml s^{-1}, surface tension is 57.0 dyne cm^{-1} and the initial spray angle is 27°. The constant b (stagnation point) in the sheet region is measured from the photograph as shown in Figs. 8 and 11; b is equal to 0.025 m. Using the stream function [equation (3)] and measuring the location of the stationary droplet (Fig. 8), one obtains with Fig. 9

$$V_{g,z} = \frac{Aa}{3+2ab} z^2(b-z) = -4.0\,\mathrm{m\,s^{-1}}$$

$$\text{at} \quad z = 0.0153\,\mathrm{m} \quad r = 0.$$

Using this relation and iterating equations (1)–(6), the constants a and A are determined

$$a = 12.72,$$

$$A = -5.04 \times 10^5.$$

In Fig. 15, the calculated results for the water sheet region are compared with experimental measurements. The effect of air circulation within the water sheet is small for the non-condensable environment. The computed values agree with the measurements. The sheet region calculations are terminated when the breakup point is reached as given by equation (23).

To compute the droplet trajectories, the drop size distribution at breakup must be known. This is where the holographic data are used. Figure 16 is a plot of the data obtained from holographic measurements. The upper-limit curve [equations (7) and (8)] is fitted to the data; and thus

$$\bar{a} = 1.1,$$

$$\delta = 1.13,$$

$$D_m = 666\ \mu\mathrm{m},$$

are obtained. The droplet trajectories are then computed for droplets in 50 μm size increments using equations (9)–(20). The computations are performed on a PDP-11/44 computer and plotted on a Tektronix

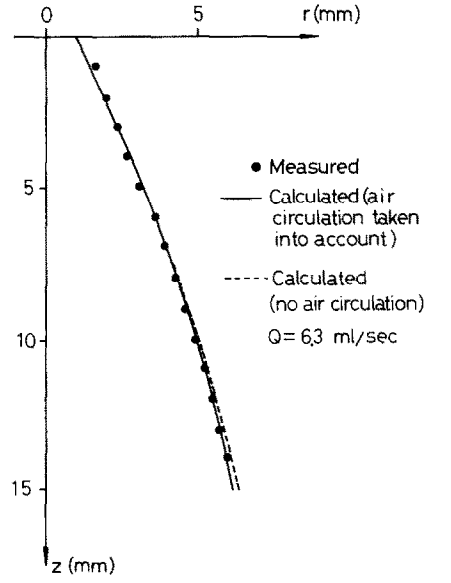

FIG. 15. Effect of internal airflow on the shape of the water sheet.

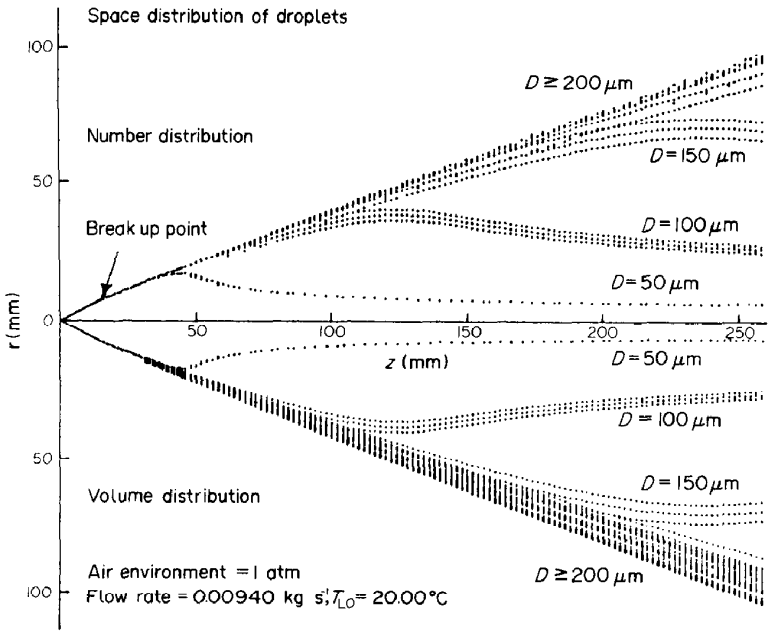

FIG. 17. Overall shape of computed spray (the diameter of droplets are grouped in 50 μm increments).

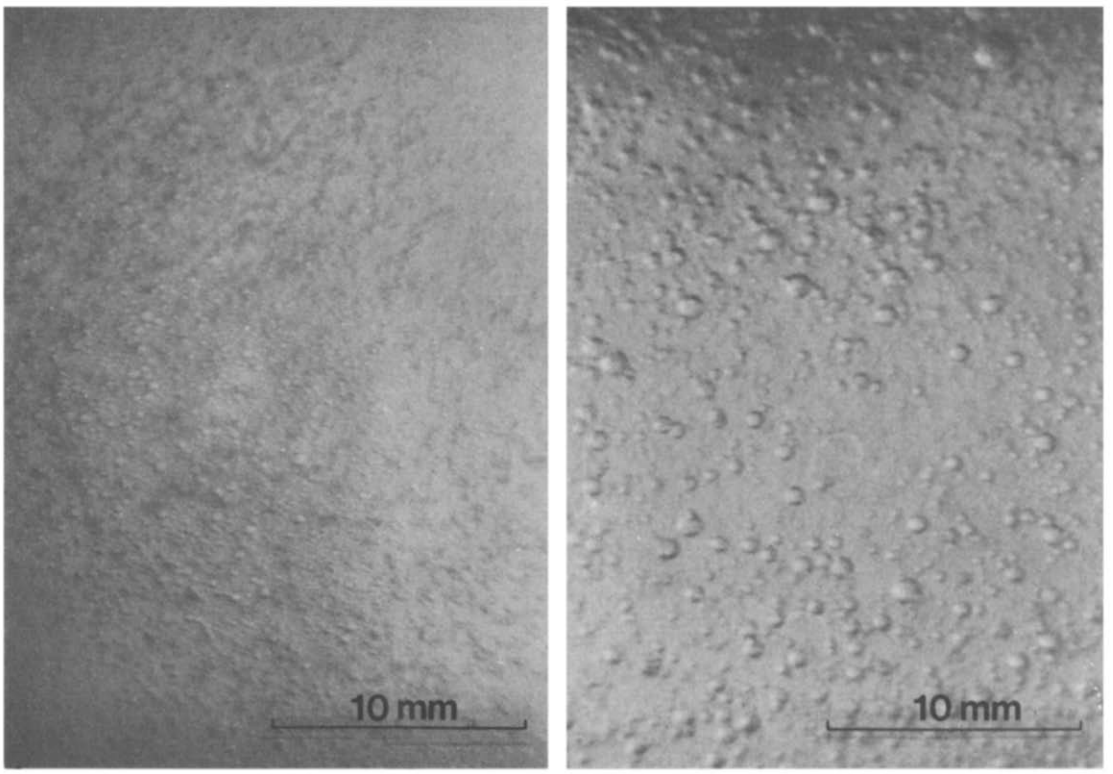

FIG. 18. Typical photograph of droplets collected at (a) center and (b) edge portions of the spray.

4052 graphics terminal. Figure 17 shows the spray behavior—starting from the nozzle, computing the sheet portion to the breakup point, and then computing the droplet trajectories. It is seen that the smaller droplets move inward; whereas the larger droplets deviate little from their original path. Figure 18 shows droplets that are captured in the oil bath about 160 mm from the nozzle. The droplets at the edge of the spray are significantly larger than those at the centerline. These photographs substantiate the computations that the small droplets migrate to the center of the spray; whereas the large droplets continue on essentially their original paths.

5. CONCLUSIONS

The behavior of a water spray in an air environment (non-condensable atmosphere) has been studied both theoretically and experimentally. The analytical model agrees with the experiments. To determine the effect of air circulation inside the sheet region, Parlange's approach was applied. For a non-condensable atmosphere and relatively short sheet portions, the gas circulation within the sheet region has little effect.

Acknowledgements—The authors wish to thank Professors Bankoff and Yuen for their helpful suggestions. The U.S. Nuclear Regulatory Commission, under Contract NRC-G-04-8L-020 provided financial support for this study.

REFERENCES

1. K. L. DeJuhasz, Dispersion of sprays in solid-injection engines, *Trans. Am. Soc. Mech. Engrs* **53,** 65–77 (1931).
2. D. W. Lee, Fuel spray formation, *Trans. Am. Soc. Mech. Engrs* **54,** 63–73 (1932).
3. D. W. Lee, A comparison of fuel sprays from several types of injection nozzles, *NACA Tech. Rep.* No. 21 (1935).
4. Y. Tanasawa and S. Toyoda, On the atomization of liquid jet issuing from a cylindrical nozzle, *Technology Rep. Tohoku Univ.* **19** (2) (1955).
5. W. E. Ranz, Some experiments on orifice sprays, *Can. J. Chem. Engng* **36** (4), 175–181 (1958).
6. R. D. Reitz and F. V. Bracco, Ultra-high-speed filming of atomizing jets, *Physics Fluids* **22** (6), 1054–1064 (1979).
7. R. P. Frazer and P. Eisenklam, Liquid atomization and the drop size of sprays, *Trans. Instn Chem. Engrs* **34,** 294–319 (1956).
8. N. Dombrowski and D. L. Wolfsohn, The atomization of water by swirl spray pressure nozzles, *Trans. Instn Chem. Engrs* **50,** 259–269 (1972).
9. S. M. DeCorso and G. A. Kemeny, Effect of ambient and fuel pressure on nozzle spray angle, *Trans. Am. Soc. Mech. Engrs* **79,** 607–615 (1957).
10. S. M. DeCorso, Effect of ambient and fuel pressure on spray drop size, *Trans. Am. Soc. Mech. Engrs*, Series A, *J. Engng Pwr* **83,** 10–18 (1960).
11. E. Giffen and A. Muraszew, *The Atomization of Liquid Fuels*, Wiley, New York (1953).
12. R. D. Reitz, Breakup regimes of a single liquid jet, AMS Report No. 1262, Princeton University (1976).
13. R. A. Castleman, The mechanism of atomization of liquids, *Bur. Stand. J. Res.* 369–376 (1931).
14. P. H. Schweitzer, Mechanism of disintegration of liquid jets, *J. Appl. Phys.* **8,** 513–521 (1937).
15. N. Dombrowski and W. R. Johns, The aerodynamic instability and disintegration of viscous liquid sheets, *Chem. Engng Sci.* **18,** 203–214 (1963).
16. N. Dombrowski and P. C. Hooper, The effect of ambient density on drop formation in sprays, *Chem. Engng Sci.* **17,** 291–305 (1962).
17. R. P. Frazer, N. Dombrowski and P. Eisenklam, Vibration as a cause of disintegration of liquid sheets, *Nature* **173,** 495 (1954).
18. N. Dombrowski and R. P. Frazer, A photographic investigation into the disintegration of liquid sheets, *Phil. Trans.* **A 247,** 101–130 (1953).
19. C. J. Clark and N. Dombrowski, An experimental study on the flow of thin liquid sheets in hot atmosphere, *J. Fluid Mech.* **64,** 167–176 (1974).
20. R. P. Frazer, P. Eisenklam, N. Dombrowski and D. Hasson, Drop formation from rapidly moving liquid sheets, *A.I.Ch.E. Jl* **8** (5), 672–680 (1962).
21. P. H. Rothe and J. A. Block, Aerodynamic behavior of liquid sprays, *Int. J. Multiphase Flow* **3,** 263–272 (1977).
22. B. J. Azzopardi, Measurement of drop size, *Int. J. Heat Mass Transfer* **22,** 1245–1280 (1979).
23. R. A. Mugele and H. D. Evans, Drop size distribution in sprays, *Ind. Engng Chem.* **43,** 1317–1324 (1951).
24. A. Lekic, R. Bajramovic and J. D. Ford, Droplet size distribution: an improved method for fitting experimental data, *Can. J. Chem. Engng* **54,** 399–402 (1976).
25. G. I. Taylor, The dynamics of thin sheets of fluid, *Proc. R. Soc. Lond.* **A 253,** 289–321 (1959).
26. J. Y. Parlange, A theory of water bells, *J. Fluid Mech.* **29** (2), 361–372 (1967).
27. R. Clift, J. R. Grace and M. E. Weber, *Bubbles, Drops and Particles*, Academic Press, New York (1978).
28. M. C. Yuen and L. W. Chen, On drag of evaporating liquid droplets, *Combust. Sci. Technol.* **14,** 147–154 (1976).
29. S. Y. Lee and R. S. Tankin, Study of liquid spray (water) in a condensable environment (steam), *Int. J. Heat Mass Transfer* **27,** 363–374 (1984).

ETUDE D'UNE PULVERISATION LIQUIDE (EAU) DANS UN ENVIRONNEMENT INCONDENSABLE (AIR)

Résumé—On propose un modèle pour décrire le comportement d'une pulvérisation d'eau dans un environnement d'air. Pour la modélisation, le brouillard est divisé en deux régions—la portion couverture et la portion des gouttelettes. La portion couverture est importante pour déterminer l'angle d'expansion. Une relation est obtenue entre la longueur et le nombre de Weber. La trajectoire calculée des gouttelettes est qualitativement vérifiée par des mesures utilisant un bain d'huile pour capturer les gouttelettes.

UNTERSUCHUNG ÜBER DAS VERSPRÜHEN VON FLÜSSIGKEIT (WASSER) IN EINE NICHTKONDENSIERBARE UMGEBUNG (LUFT)

Zusammenfassung—Es wird ein Modell vorgestellt, welches das Verhalten von in Luft versprühtem Wasser beschreibt. Zur Modellbildung wird die zerstäubte Flüssigkeit in zwei Bereiche eingeteilt—ein Grenzflächengebiet und ein Tröpfchengebiet. Das Grenzflächengebiet ist wichtig für die Bestimmung des Sprühwinkels. Es ergibt sich eine Beziehung zwischen der Länge der Grenzfläche und der Weber-Zahl. Die berechnete Flugbahn der Tröpfchen wurde durch Messungen, bei denen die Tröpfchen in einem Ölbad aufgefangen wurden, qualitativ bestätigt.

ИЗУЧЕНИЕ РАСПЫЛЕНИЯ ЖИДКОСТИ (ВОДЫ) В НЕКОНДЕНСИРУЕМОЙ СРЕДЕ (ВОЗДУХЕ)

Аннотация—Предложена модель, описывающая распыл воды в воздушной среде. С целью моделирования распыл делился на два участка: плоский и капельный. Плоский участок важен для определения угла распыления. Получена зависимость длины плоского участка от числа Вебера. Рассчитанная траектория капель подтверждена качественно путем измерений, проведенных с использованием масляной ловушки.